Biomedical Signal Processing and Control 74 (2022) 103455

Contents lists available at ScienceDirect

Biomedical Signal Processing and Control

journal homepage: www.elsevier.com/locate/bspc

Optimization of VGG16 utilizing the Arithmetic Optimization Algorithm for early detection of Alzheimer's disease

N. Deepa *, S.P. Chokkalingam

Department of Computer Science and Engineering, Saveetha School of Engineering, Saveetha Institute of Medical and Technical Sciences, Chennai, Tamilnadu, India

ARTICLE INFO

Keywords:
Alzheimer's disease
ADNI dataset
An adaptive ROI
VGG-16
Arithmetic Optimization Algorithm

ABSTRACT

Early detection and prevention of Alzheimer's disease (AD) is an important and challenging task. Determining a precise and accurate diagnosis of Alzheimer's disease in its early stages is the most significant challenge. As a result, various research for the early detection of Alzheimer's disease was conducted. However, these techniques have a number of drawbacks, including higher computational costs, failure to incorporate data from multiple modalities, performance degradation due to data distributions between training and testing data, inability to record brain affected regions, longer processing time, etc. To tackle these issues, we proposed Optimized VGG-16 architecture using Arithmetic Optimization Algorithm (Optimized VGG-16 using AOA) for AD classification. Three major components are involved in this study such as pre-processing, segmentation, and classification. The CAT12 toolkit is used to process the format of T1-weighted MRI images during pre-processing. The image enhancement techniques normalize the uneven light distribution in which the linear contrast stretching enhances the image contrast level. Finally, an Optimized VGG-16 using AOA effectively classifies the AD classes such as normal, mild dementia (severe cognitive decline), and late dementia (very severe cognitive decline) classes. The dataset images are chosen from Alzheimer's disease Neuroimaging Initiative (ADNI), the Open Access Series of Imaging Studies (OASIS) dataset, and Single Individual volunteer for Multiple Observations across Networks (SIMON) databases. The experimental investigations provided superior classification performances than other existing methods.

1. Introduction

One of the common prevailing kinds of dementia is Alzheimer's disease (AD). The cognitive function, progressive memory impairment with the disorder of irreversible brain degeneration is AD. Around 5% of those over the age of 65 believe they have AD. By 2050, an estimated 0.64 billion people would have been diagnosed with AD [1]. The brain cells are damaged, resulting in mental function loss and memory loss in persons. At first, AD affects the portion of the brain that controls memory and language. There is complexity and confusion in writing, reading, or speaking with memory loss as the major symptoms of AD patients [2]. The patients may not distinguish their family members and they often forget about their life.

Mild, very mild, and moderate are the three major classes involved in AD. The diagnosis of AD patients is inexact and difficult before they reach the moderate AD stage [3]. Neurobiological and physical examinations are required to correct medical evaluation of AD. For AD diagnosis, the physicians utilize brain MRI. From normal control (NC) to dementia, the transitional state is Mild cognitive impairment (MCI). According to the MCI stage, the major task is presymptomatic AD diagnosis. While curative treatment becomes available, it becomes even more urgent and crucial [3].

The quantitative measurement of metabolic activities of bain is provided with the help of Fluorodeoxyglucose positron emission tomography (FDG-PET) [4]. The cerebral sectional metabolic deviation in AD has occurred prior to the change in the onset of the structural brain. AD is associated with cognitive and functional impairment in patients who have a regional metabolic deviation. For presymptomatic detection of AD, the potential tool FDG-PET is used. The presymptomatic detection of AD demonstrated limited success based on the existing studies' efforts to detect the subjects [5]. Based on the previous study, the progressive MCI is identified by developing automated tools that demonstrated limited accuracy of less than 80%.

For AD disease screening and tracking, the likelihood functions with regression models are introduced in the existing works. Compared to the existing studies, the support vector machine (SVM) deep neural network

* Corresponding author.
E-mail addresses: deepa23narayanan@gmail.com (N. Deepa), cho_mas@yahoo.com (S.P. Chokkalingam).

https://doi.org/10.1016/j.bspc.2021.103455
Received 18 June 2021; Received in revised form 1 November 2021; Accepted 16 December 2021
Available online 10 January 2022

(DNN) and convolutional neural network (CNN) demonstrated optimal and excellent performances. The AD-related progression patterns are recognized by applying the deep learning neural network (DNN) [6]. Machine learning methods were recently initiated in which several techniques are based on computer vision [7,32,33]. Based on multi-channel EEG, author [29] constructed multiple networks in which every ECG channel has the ability to change keen on the one-layer network. The features were selected with the help of feature selection techniques. For Alzheimer's disease identification, Yu et al. [30] suggested supervised network-based fuzzy learning of EEG signals. In AD identification, the most effective factors are the clustering coefficient and local efficiency [35–40].

Based on the Latent Factor of Multi-Channel EEG, Li et al. [31] examined feature extraction and identification of Alzheimer's disease. The properties of the power spectrum were investigated, as well as the dominating frequency of the two groups. The latent components were projected using a three-dimensional state space. Existing methodologies have a few drawbacks, such as higher computational costs, failure to include data from different modalities, data distributions between training and testing data degrade performance, inability to capture brain affected regions, longer processing time, etc. To deal with these problems, we proposed an Optimized VGG-16 using Arithmetic Optimization Algorithm (Optimized VGG-16 using AOA) for AD classification. The classification section describes the study's novelty. The drawbacks of the VGG-16 model are improved by utilizing AOA, in which the optimal parameter is provided to the VGG-16 model during classification to optimize the dropout rate and batch size. The major role of this article is summarized as below:

- During pre-processing, the CAT12 toolkit is used to process the format of a T1-weighted MRI image. The uneven light distribution is normalized thereby the image contrast level is enhanced via linear contrast stretching.
- An adaptive ROI model segments the brain image nodules. The segmentation model performance is impacted by adding redundant information into the ROIs.
- The AOA parameters are run multiple times, yielding addition, subtraction, multiplication, and division operations, with the optimal parameter being provided to the VGG-16 model to optimize the dropout rate and batch size.
- The optimal VGG16 architecture has a low computing cost, can use numerous datasets, handles data imbalance issues, and has a low computational time.
- An optimized VGG-16 using AOA categorizes normal, mild dementia, and late dementia corresponding to the AD classes.

The rest of the paper is arranged as: Section 2 summarizes the related works. The proposed work is discussed in section 3. The experimental investigations are discussed in section 4. Finally, section 5 concludes the article.

2. Review of related works

For AD detection, Liu et al. [8] introduced Multi-Modality Cascaded Convolutional Neural Networks (MC-CNN). From local CNNs, the learned features are combined using the upper high-level CNNs set. From multiple imaging modalities, the multimodal and generic multi-level features are learned automatically. The MC-CNN method requires no image segmentation model but it yields 93.26% classification accuracy, nevertheless, the computational cost is higher. Based on analysis of FDG-PET images, the Multiscale Deep Neural Networks (MDNN) was proposed by Lu et al. [9] for AD diagnosis in which the image data were chosen from Alzheimer's disease Neuroimaging Initiative (ADNI) database. This MDNN model exceeds the accuracy of the classification by 82,51%, compared with previous approaches. This model delivers stable and robust performance but is unable to incorporate the data from multiple modalities.

Table 1
Literature survey.

Reference	Nam of the methods	Dataset used	Merits	Demerits
Liu et al. [8]	MC-CNN	ADNI database	Accomplishing 93.26% accuracy but it requires no image segmentation	Higher computational cost
Lu et al. [9]	Multiscale (MDNN)	ADNI dataset	Stable and robust performance	Failed to incorporate data from multiple modalities
Islam et al. [10]	e-CNN	OASIS dataset	Effectively identifies the different stages of AD	Not suitable for other AD datasets
Liu et al. [11]	DM^2L	ADNI dataset	Discriminative landmarks effectively-identified	The performance is degraded due to data distributions among the training and testing data
Puente-Castro et al. [12]	DL models	OASIS and ADNI datasets	Higher detection performance with low computational complexity	Unable to record the brain affected regions
Marzban et al. [13]	CNN	ADNI datasets	Better accuracy values	Takes higher processing time

For AD diagnosis, Islam et al. [10] introduced an ensemble system of deep convolutional neural networks (e-CNN). The Open Access Series of Imaging Studies (OASIS) dataset provided the experimental data. The early-stage diagnosis performance of AD using the e-CNN model is superior to other existing methods. The e-CNN model effectively identifies the different stages of AD but is not suitable for other AD datasets. Liu et al. [11] proposed Deep Multi-task Multi-channel Learning (DM^2L) to diagnose AD. The demographic information of subjects and MR imaging data provided clinical score regression in which the multiple-image patches are extracted. The discriminative landmarks are effectively-identified, since, the classification performance is degraded due to data distributions among the training and testing data.

Puente-Castro et al. [12] proposed deep learning (DL) techniques for AD diagnosis. In order to achieve accurate outputs, transfer learning (TL) techniques are used to conduct the experiments. For the experimental investigation, the OASIS and ADNI datasets from Sagittal MRIs image are employed. The traditional horizontal plane MRI, when compared to earlier studies, yielded satisfactory results. Because of the phenotypic manifestation, the challenging stages are discovered earlier, resulting in reduced data augmentation and the usage of TL approaches. Despite the fact that the experimental findings showed improved detection performance with minimal computational complexity, it was unable to record the brain-affected regions.

The convolutional neural networks (CNN) using diffusion tensor images were suggested by Marzban et al. [13] for AD detection. The input images are gray-matter (GM) volumes and diffusion maps respectively. The AUC of 0.84 and 0.94 were produced by using stacked mean diffusivity (MD) and GM volume thereby adopting ten-fold cross-validation. From various imaging modalities, this CNN explained the data impacts. This method took higher processing time but it provides 93.5% accuracy. The literature survey is summarized in Table 1.

3. Proposed methodology

This section proposed efficient models for AD classification. The proposed model includes three major sections namely pre-processing, segmentation, and classification in which the overall architecture of

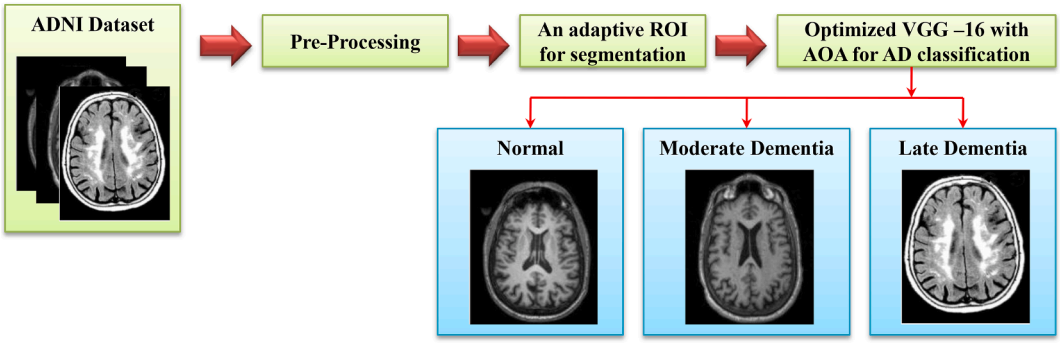

Fig. 1. Overall architecture of proposed methodology.

the proposed work is delineated in Fig. 1. Our proposed methodology is implemented in a medical decision support module which helps to provide Alzheimer's disease diagnosis. Initially, the patients' records are given as input to the proposed model, which diagnoses Alzheimer's disease based on several parameters, and the findings of the diagnosis are submitted to the doctor for final verification. If the suspected patient's results are as expected, they are at risk of developing Alzheimer's disease, but if no abnormalities are found, the patient's results are normal.

3.1. Pre-processing

Pre-processing is the major step involved in medical image training and testing for the proposed model. The default value setting with the CAT12 toolkit is used to process the format of the T1-weighted MRI image. After processing, the pre-processing steps involve image smoothening, extraction of the skull, MNI space form registration [14]. Because of the poor brightness created by visual equipment, MRI images show deterioration such as low variation. The image enhancement model is used to improve MRI images across a wide range of intensities in order to overcome this problem.

Because of the non-linear light intensity recognized as noise, some undesirable information is added to the image during the image acquisition process. The overall accuracy performance of the image processing is affected due to non-linear light intensity [15]. The image enhancement techniques normalize the uneven light distribution and the non-linear light was established because of improper lens slit setting of the scanning devices. The contrast stretching increases the dynamic light intensity ranges due to the image outputs thereafter the procedure consists of suitable light distribution and enhanced contrast. The linear contrast stretching enhances the image contrast level.

3.2. Segmentation using an adaptive ROI (A-ROI) model:

For the next slice to search for the presence of nodule, the ROI is dynamically selected using an adaptive ROI model. The ROI position is adjusted using nodule mask and ratio maintenance among the ROI (*i.e.* below the threshold (T)) and nodule area are the major objectives of this method. The nodule penetration search stages into adjacent slices are described in Algorithm 1. The user provides the segmentation of nodule is executed on the manual ROI. In the predicted mask, identify the margins thereby adjusting the size and position of ROI thereafter attaining predicted nodule segmentation [16].

Algorithm 1: The brain nodule segmentation using A-ROI

Initialization of user-provided ROI
Given ROI with the segmentation of nodule in current slice (R_j)
While $a_{M_j} > 0$ **do**
$\Delta E_A = E_L - E_P$
$\Delta E_B = E_T - E_C$
$A_1^{'} = A_1 + \Delta E_A$

(*continued on next column*)

(*continued*)

Algorithm 1: The brain nodule segmentation using A-ROI

$A_2^{'} = A_2 + \Delta E_A$
$B_1^{'} = B_1 + \Delta E_B$
$B_2^{'} = B_2 + \Delta E_B$
If
$\frac{a_{M_j}}{a_{ROI_j}} > P_T$
Then
$a_{ROI_j+1} = \frac{a_{M_j}}{P_T}$
$\Delta a = a_{ROI_{j\pm1}} - a_{ROI_j}$
$E_S = Ceil(\sqrt{\Delta a}/2)$
$A_1^{'} \leftarrow A_1^{'} - E_s$
$A_2^{'} \leftarrow A_2^{'} + E_s$
$B_1^{'} \leftarrow B_1^{'} - E_s$
$B_2^{'} \leftarrow B_2^{'} + E_s$
End If
The next slice movement: $s_j \leftarrow s_{j\pm1}$
ROI updated with the nodule segmentation in the next slice
End While

From Algorithm 1, the nodule area of j^{th} current slice, ROI in j^{th} current slice, and the next $(j \pm 1)^{th}$ slice is indicated as a_{M_j} , a_{ROI_j} and $a_{ROT_{j\pm1}}$. The bottom, top, left and right margins of the predicted mask are denoted as E_C , E_T , E_L and E_R. Along with the A and Baxis, the differentials in the margins are provided using ΔE_A and ΔE_B. According to the current ROI, the beginning and ending coordinate points are A_1, A_2 and B_1, B_2. Based on the updated ROI in the next $(j \pm 1)^{th}$ slice, the beginning and ending coordinate points are $A_1^{'}, A_2^{'}$ and $B_1^{'}, B_2^{'}$.

An optimal ROI size selection is determined using Algorithm 1 thereafter detecting the next ROI position. A similar length present on every side of the calculated ROI. The selected ratio threshold (P_T) with the constant value is smaller when the method retains the ratio among a_{ROI} and a_M. Within the two adjacent slices, the maximum feasible movement of the nodule is directly linked.

$$P_T \alpha \frac{1}{S_{lice} T_{hickness}} \tag{1}$$

Data validation determines the optimal P_T value.

$$P_T \leqslant \frac{a_M}{a_{ROI}} \tag{2}$$

where, $P_T \in (0, 1)$ and a_{ROI} of minimal feasible value is similar to a_M. The segmentation model performance is impacted by adding redundant information into the ROIs as described in Algorithm 1. The algorithm computes the differential (Δa) between the required area of ROI next slice and the current area of ROI. For ROI coordinate update, the required size is obtained by utilizing Δ. An adaptive ROI and constant ROIs are determined. It fails to cover the area of nodule available in other slices while the ROI remains closer to the initial slice nodule. The

segmentation model performance is impacted by adding redundant information into the ROIs. The ROI without the requirement to other slices is selected and also the ROIs are selected optimally. The segmentation model performance is enhanced by facilitating the remainder of slices. Deep Residual U-Net architecture [17] is used along with an adaptive ROI thereby performing better performance in terms of brain nodule segmentation.

Within each ROI, the patch sizes to have 500, 1000, and 1500 voxels are selected. For the whole brain, several smaller units of various image sizes output to the total number of patches such as 343, 705, and 1488. The sufficient brief information determines the patch size and the restricted number of data samples are considered by neglecting too large a feature dimension. According to the ROI size, the amount of voxels in every patch is predefined. At similar scales across every ROI in the brain, the uniform patch size density is provided for various ROIs along with the brain guiding to the aggregation of the signal [9]. The metabolism feature extracts the image intensities in each patch.

3.3. Classification

In this study, we have used Convolutional Neural Network in terms of VGG16 with Arithmetic Optimization Algorithm (Optimized VGG-16 using AOA) for the classification AD such as normal, mild dementia (severe cognitive decline), and late dementia (very severe cognitive decline).

3.3.1. Convolutional neural network

The VGG-16 is the major base of CNN. The Visual Geometry Group (VGG) trains and designs object recognition in which the most important deep convolutional neural network is VGG-16 [18]. This network is known based on the simple architecture and good performance despite its around 160 million parameters. In 2015, the Google research team develops the network Inceptionv3. The higher computational cost associated with CNN is overcome using a pre-trained architecture such as VGG16 [19]. In this study, the convolution, pooling, fully connected and output layers are the four major components involved in CNN.

A. Convolutional layer: The most significant component in CNN is a convolutional layer. The convolution-oriented process transforms the input into an output. The volumetric structure shows both input and output. The fixed width and height with planes compose the input volume. The depth D is defined as the number of planes. The number of M planes with the volume structure present in the convolutional layer. The number of kernels or filters with their smaller size (K_s) defines each plane. The weight with the size of the filter is 3×3. Y_k is the matrix value with respect to the k^{th} input plane.

The parametric weight is w_{kl}. Over the k^{th} input plane, the two-dimensional matrix $w_{kl} * Y_k$ is produced using the convolution of this filter [20]. The activation function F transforms the result and the bias function b_l.

$$X_l = F\left(b_l + \sum_{k=1}^{D} w_{kl} * Y_k\right); \quad l = 1, ..., M \tag{3}$$

The feature map resulting matrix X_l. The feature map is M. In the current CNN architecture, the activation function is ReLU. When keeping each positive input similar, it changes all the values of inputs to zero.

$$F(y) = Max(0, y) \tag{4}$$

The convolutional layer output applies the ReLU function. The classification accuracy and the network learning speed increased.

B. Pooling layer: The feature map size is reduced using a pooling layer after each block of a layer or convolutional layer. When neglecting irrelevant details, the important information is preserved. The model sensitivity to distortions and shifts are reduced the feature positions within the input images [21]. The stride (s) and the squared section of the feature map size (F) are the two important parameters to define pooling.

Table 2
Summary ofVGG-16 implementation architecture.

Layers	M- number of planes (filters)	Size of the filters	Max pooling
$2 \times conv2D$	64	3×3	s = 2 and F = 2
$2 \times conv2D$	128	3×3	s = 2 and F = 2
$3 \times conv2D$	256	3×3	s = 2 and F = 2
$3 \times conv2D$	512	3×3	s = 2 and F = 2
$3 \times conv2D$	512	3×3	s = 2 and F = 2
1000 nodes fully connected with softmax activation			
4096 fully connected nodes			

The s = 2 and F = 2 with five pooling layers present in a VGG-16. Over the whole feature map, the two pixels steps with each 2×2 pixel apply the pooling layer. The VGG-16 implementation architecture is summarized in Table 2. The blocks organize 13 convolutional layers in which it composes in the VGG-16 network [19].

C. Fully connected and output layer: Obtain the feature map set after the pooling and successive convolutions layers. The input–output operation performed using each neuron of the fully connected layer is as shown below:

$$Z = F\left(b + \sum_{j}^{n} w_j Y_j\right) \tag{5}$$

Hence, the neuron weight and the input features are Y_j and w_j. The fully connected layer output is Z. The softmax activation function is delineated as below:

$$F(x_j) = Softmax(x_l) = \frac{e^{(x_l)}}{\sum_{k=1}^{8} e^{(x_k)}}, \quad for \quad l = 1, ..., 8 \tag{6}$$

The probability distribution result is obtained by applying the output layer of each node's results. In this study, we have used three output neurons to classify the AD classes.

3.3.2. Formulation of Arithmetic Optimization Algorithm (AOA)

Randomly generated a candidate solution set with population-oriented methods begins with the enhancement process. The optimization rule set incrementally improves the generated set of solutions in which the specific objective function evaluates it. For the given problem, the global optimization algorithm obtains the probability [22]. The optimization model has two major classes in the realm of population-based optimization techniques: exploration and exploitation. During the exploration stage, the latter is the enhancement of obtained solution's accuracy. According to Arithmetic Optimization Algorithm (AOA), the following sub-sections delineate the diversification (exploration) and intensification (exploitation). Addition, subtraction, multiplication, and division are the major arithmetic operators.

(i) Inspiration

Along with algebra, geometry, and analysis, one of the significant sections of modern mathematics is a fundamental component of number theory called arithmetic. From few candidate solution sets, the best element subjected to a particular criterion is determined using an AOA as the mathematical optimizations.

(ii) Initialization stage

Equation (7) shows the candidate solution set (Y) in AOA. In each iteration, the best-obtained solution considers the best candidate solution.

Algorithm 2: AOA pseudo-code

Input: Initialization of AOA parameters with the maximum number of iterations
Output: Obtain the best solution
While ($c\_iteration < M\_iteration$) **do**
Evaluate the fitness function
Obtain the optimal solution if it findsany optimal so far

(*continued on next page*)

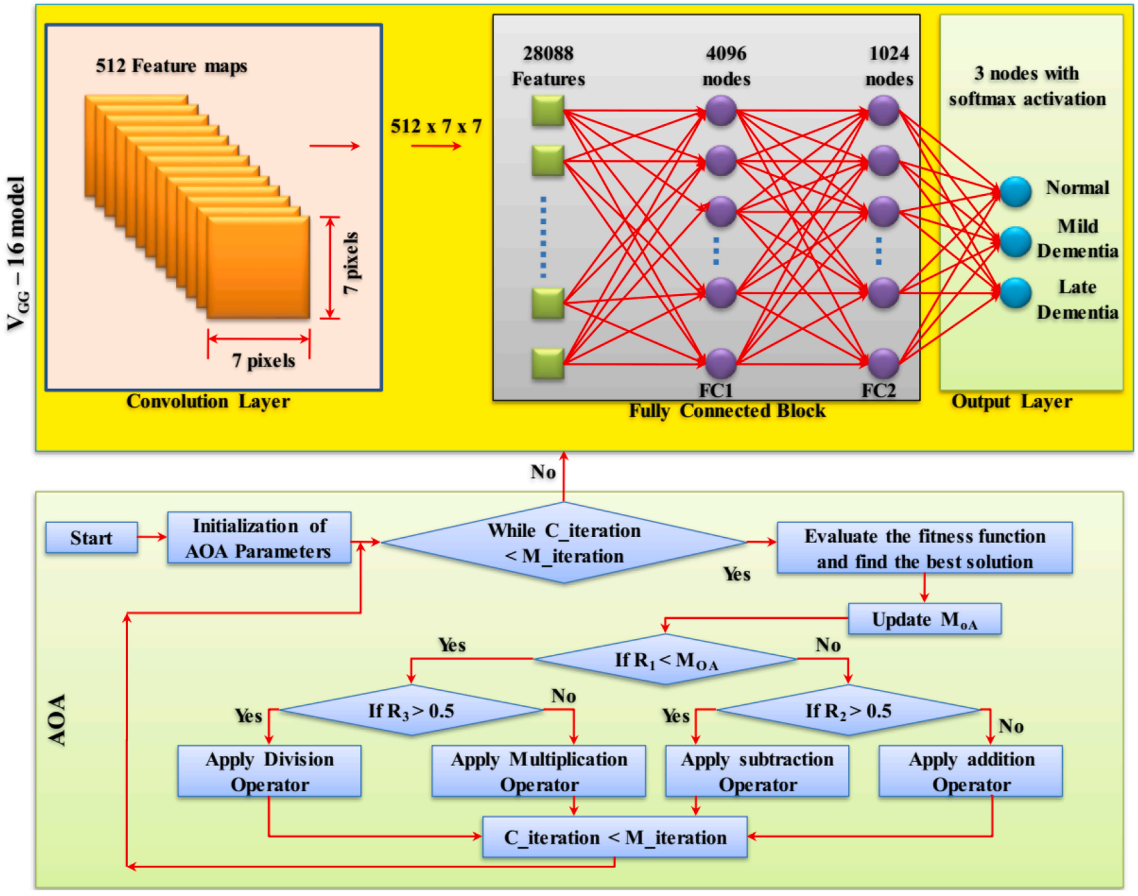

Fig. 2. An optimized VGG-16 using AOA model for AD classification.

(*continued*)

Algorithm 2: AOA pseudo-code

Equation (2) update the value of M_{OA}
Equation (4) update the value of M_{OA}
For ($j = 1$ *to* $s_{olution}$) **do**
  For ($j = 1$ *to* $s_{olution}$) **do**
The random values R_1, R_2,and R_3 generated between [0,1]
If $R_1 > M_{OA}$
  Then
  Diversification stage
  If $R_2 > 0.5$
  Then
  The division math operator is applied
  Equation (3) updates the j^{th} solution position
  Else
  The multiplication math operator is applied
  Equation (3) updates the k^{th} solution position
  End If
Else
Intensification stage
  If $R_3 > 0.5$
  Then
  The subtraction math operator is applied
  Equation (5) updates the j^{th} solution position
  Else
  The addition math operator is applied
  Equation (5) updates the k^{th} solution position
  End If
End If
End For
End For
($c\_iteration < c\_iteration + 1$
End While

$$Y^{i} = \begin{bmatrix} y_{1,1} & \cdots & \cdots & y_{1,i} & y_{1,m-1} & y_{1,m} \\ y_{2,1} & \cdots & \cdots & y_{2,i} & y_{2,m-1} & y_{2,m} \\ \cdots & \cdots & \cdots & \cdots & \cdots & \cdots \\ \vdots & \vdots & \vdots & \vdots & \vdots & \vdots \\ y_{M-1,1} & \cdots & \cdots & y_{M-1,i} & \cdots & y_{M-1,m} \\ y_{M1} & \cdots & \cdots & y_{M,i} & y_{M,m-1} & y_{M,m} \end{bmatrix} \tag{7}$$

The search stage is selected before the AOA initializes working. Equation (8) calculates the math optimizer accelerated (M_{OA}) function.

$$M_{OA}(c\_iteration) = Minimum + c\_iteration \times \left(\frac{Maximum - Minimum}{M\_iteration}\right) \tag{8}$$

At t^{th}iteration, the function value is denoted as $M_{OA}(c - iteration)$ thereby maximum and minimum iteration is calculated.

(iii) Diversification stage:

We introduced the AOA of diversification or exploration behavior in this section. The high distributed value is obtained using multiplication or division operator based on the arithmetic operators. Based on division and multiplication, the best solution is determined by exploring AOA exploration operators [23]. The arithmetic operator's behavior is simulated by employing the simplest rule. Equation (9) illustrates the position update of the exploration stage.

$$y_{j,k}(c.iteration+1) = \begin{cases} B(y_i) \div (M_{OA} + \delta) \times ((U_i - L_i) \times \alpha + L_i) & R_2 < 0.5 \\ B(y_i) \times M_{OA} \times ((U_i - L_i) \times \alpha + L_i) & otherwise \end{cases} \tag{9}$$

In the next iteration, the j^{th} and k^{th} solution position is denoted as $y_{j,k}(c - iteration)$. The small integer is δ with the controlling parameter is α. The j^{th} position of upper and lower bound is U_i and L_i .

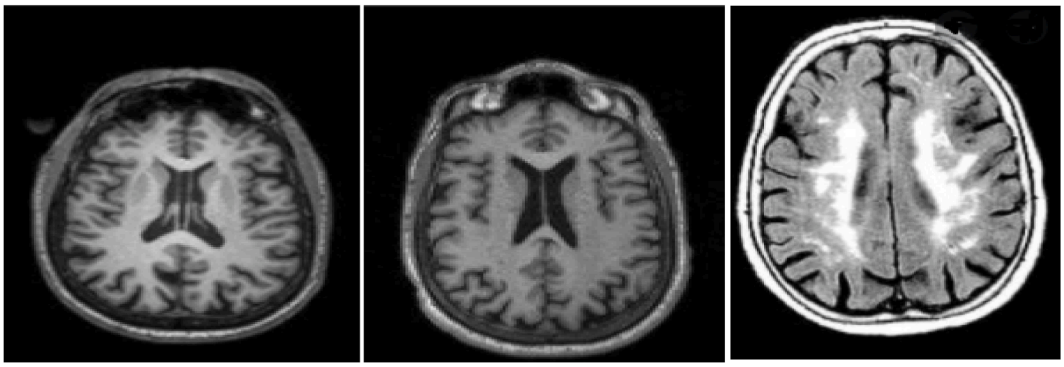

(a) (b) (c)

Fig. 3. Sample images based on ADNI database, (a) Normal, (b) Mild dementia, and (c) Late dementia.

$$M_{OA}(c\_iteration) = 1 - \frac{c\_iteration^{1/\beta}}{M\_iteration^{1/\beta}} \tag{10}$$

At the t^{th} iteration, the function value is expressed as $M_{OA}(c - iteration)$. Further, the sensitive parameter is β.

(iv) Intensification stage:

Higher dense outputs are obtained using addition or subtraction of arithmetic operator. Because of low dispersion, addition and subtraction is easily the target approach. After a little iteration, deduce the near-optimal solution during the detection of exploration search. Equation (11) delineates the exploitation stage.

$$y_{j,k}(c\_iteration + 1) = \begin{cases} B(y_i) - M_{OA} \times ((U_i - L_i) \times \alpha + L_i) & R_3 < 0.5 \\ B(y_i) \times M_{OA} \times ((U_i - L_i) \times \alpha + L_i) & otherwise \end{cases} \tag{11}$$

Utilize the search operator of exploitation to avoid getting trapped in the local search area. The random values R_1, R_2, and R_3 were generated between 0 and 1 intervals. The optimal solution is obtained by assisting the exploitation search stage. Algorithm 2 describes the AOA pseudo-code.

3.3.3. Optimized VGG-16 using AOA for AD classification

The VGG-16 in CNN met a few shortcomings in the case of parameter optimization such as weights, dropout rate, and batch size with overfitting and more training time reduction. Hence, we used Arithmetic Optimization Algorithm (AOA) to boost up the performance of the VGG-16 model. The AOA parameters with a maximum number of iteration are carried out thereby the addition, subtraction, multiplication, and division operations are performed in which the optimal parameter is fed to the VGG-16 model to optimize the dropout rate and batch size [23,24]. An optimized VGG-16 using the AOA model for AD classification is delineated in Fig. 2. Therefore, the optimized VGG-16 using the AOA model accurately classifies the classes of AD such as normal, mild dementia, and late dementia respectively.

4. Result and discussion

The Python, Keras, and Tensor Flow on Linux X86-64 machine with NVIDIA GeForce GTX 770, 16 GB RAM, and AMD A8 CPU implement the proposed model [10,25]. The optimized parameters such as learning rate of 0.001, mini-batch size of 6, and 0.06 wt decay are used in this study. Based on AOA, there are 100 epochs used. Various experimental analyses were carried out to evaluate the proposed model performance.

Table 3
Details about the training and testing images.

Name of the classes	Total image	Training image	Testing image
Normal	229	153	76
Mild dementia	398	266	132
Late dementia	192	128	64

4.1. Dataset explanation

The experimental images were chosen from the database of Alzheimer's disease Neuroimaging Initiative (ADNI) [26], Open Access Series of Imaging Studies (OASIS) dataset [10], and Single Individual volunteer for Multiple Observations across Networks (SIMON) dataset [34]. In the Canada and USA, the participants across 57 sites recruit the North American cohort. The progression of early AD and mild cognitive impairment (MCI) is measured by combining neuropsychological and clinical assessments with other biological markers [27]. The sample of dataset images is illustrated in Fig. 3.

The ADNI dataset consists of a total of 819 images. This study incorporates 229 normal images, 192 late dementia images, and 398 mild dementia images. 70% of images were used for training and the remaining 30% for testing [28]. The details about training and testing images are delineated in Table 3.

4.2. Performance measures

In this study, we have used various kinds of evaluation measures including Accuracy (*A*), Specificity (*Spec*), Sensitivity (*Sen*), Precision (*P*), Recall (*R*), and F-measure to verify the proposed model performance. The following equations explain each evaluation criteria. The T_{pos} and T_{neg} are true positive and true negative. Further, the false positive and false negative is defined as F_{pos} and F_{neg}.

$$A_{ccuracy} = \frac{T_{neg} + T_{pos}}{T_{pos} + T_{neg} + F_{pos} + F_{neg}} \tag{12}$$

$$Sen = \frac{T_{pos}}{T_{pos} + F_{neg}} \tag{13}$$

$$Spec = \frac{T_{pos}}{T_{neg} + F_{pos}} \tag{14}$$

$$P = \frac{T_{pos}}{T_{pos} + F_{pos}} \tag{15}$$

$$R = \frac{T_{pos}}{T_{pos} + F_{neg}} \tag{16}$$

Table 4
Pre-processing results.

Parameters	Without pre-processing	With pre-processing
Training rate	96.11 %	97.89%
Test rate	89.34%	92.34%

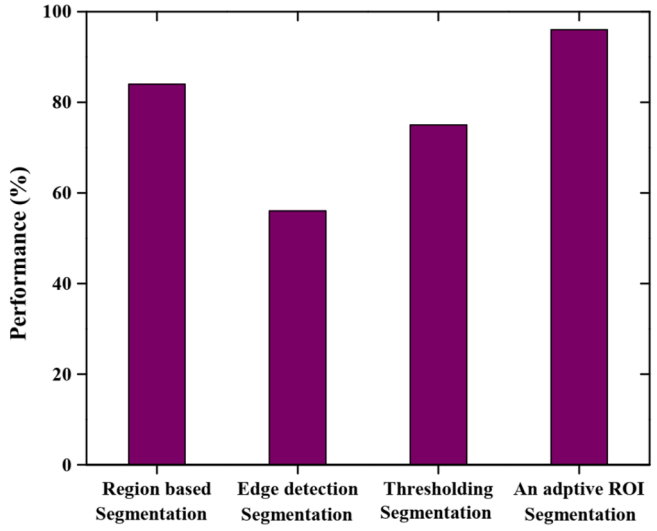

Fig. 4. State-of-art result of segmentation.

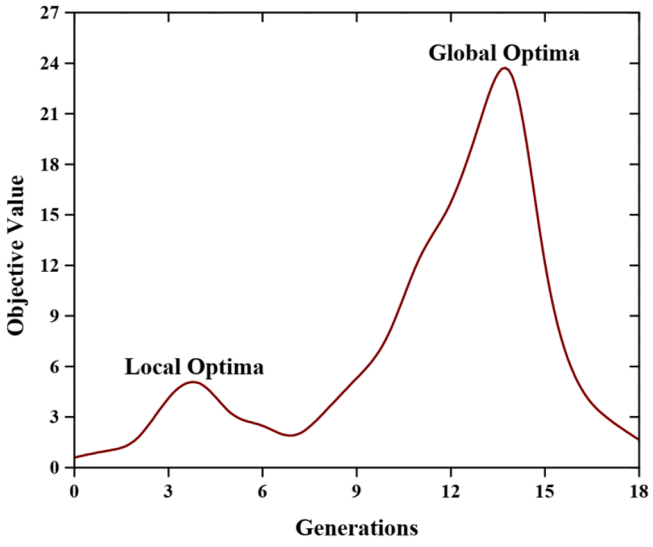

Fig. 7. Local and global optima performance analysis of AOA.

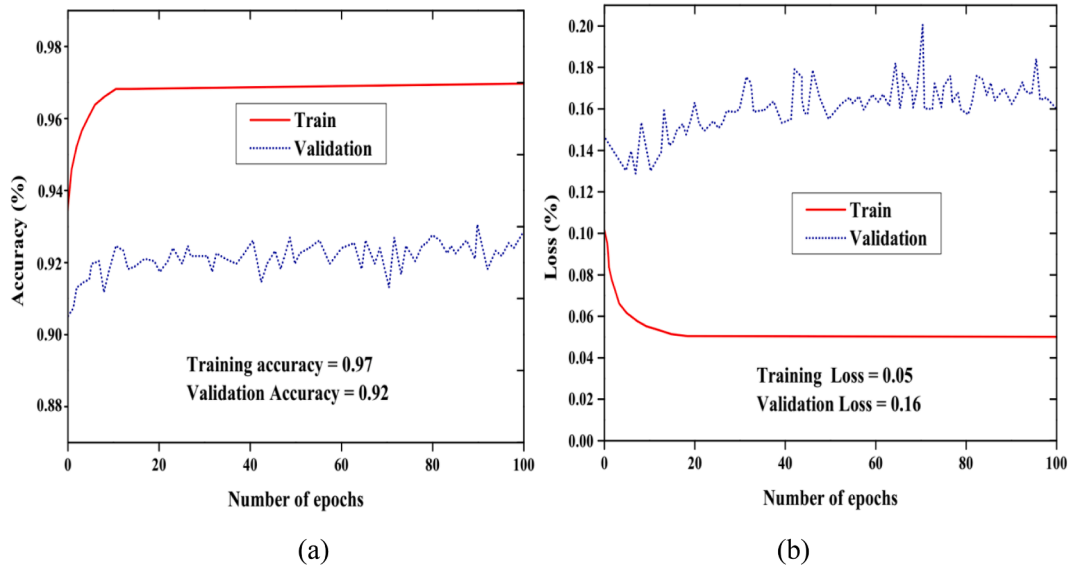

Fig. 5. Performance assessment, (a) Accuracy and (b) loss.

True class	Predicted class		
	Normal	**Mild dementia**	**Late dementia**
Normal	97%	0	3%
Mild dementia	4%	96%	0
Late dementia	0	5%	95%

Fig. 6. Confusion matrix assessment based on classifier performance.

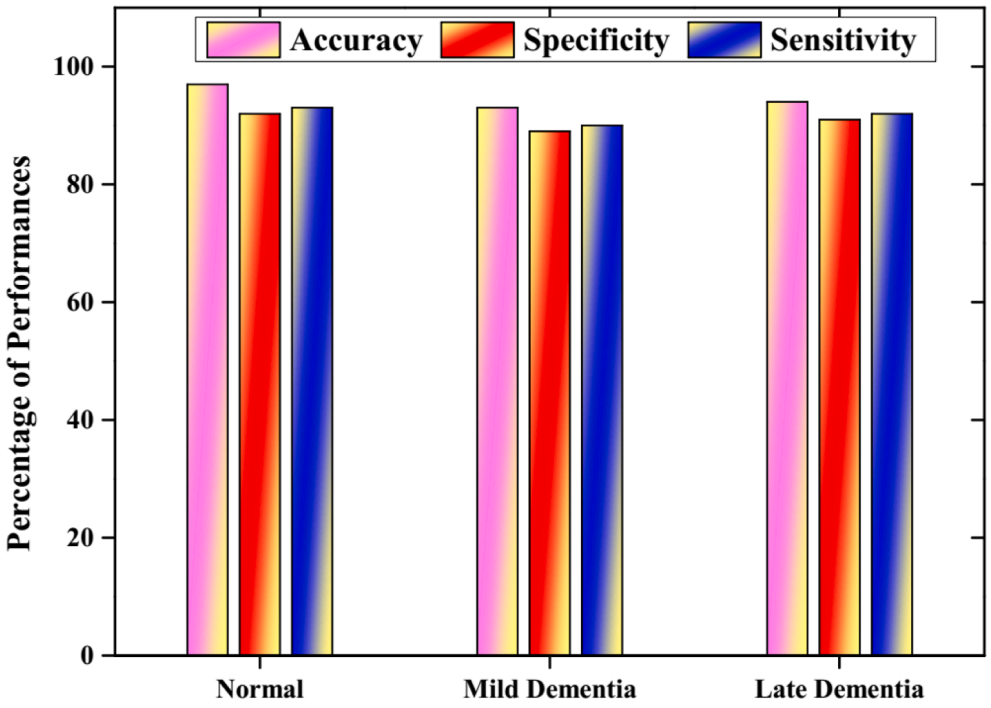

Fig. 8. Performance assessment of various classes.

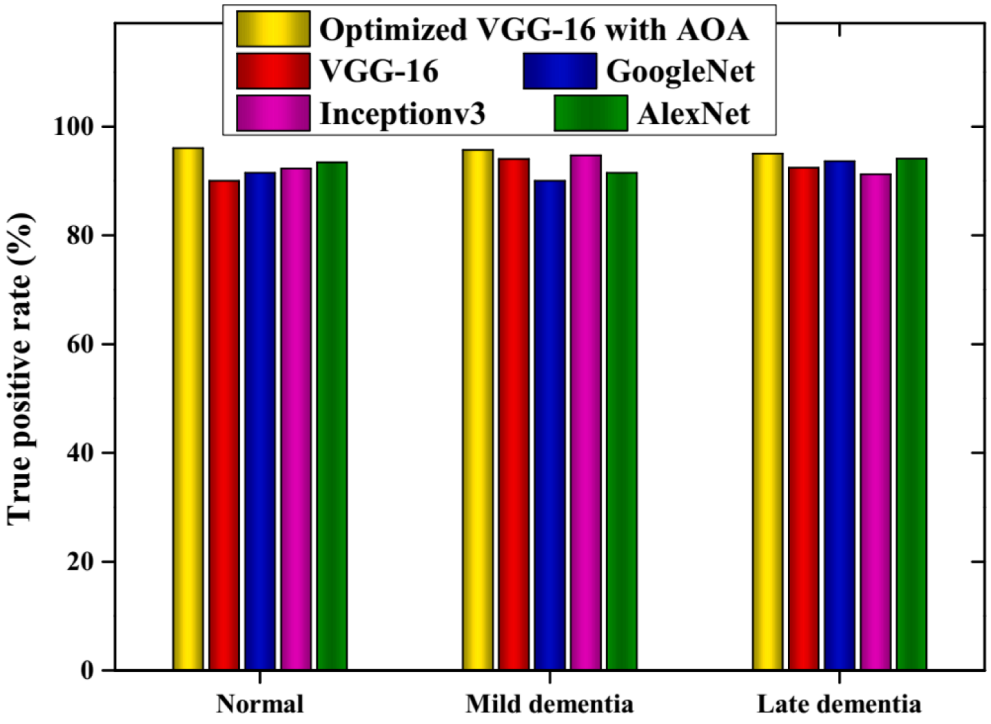

Fig. 9. State-of-art comparison of classification based on the evaluation measures.

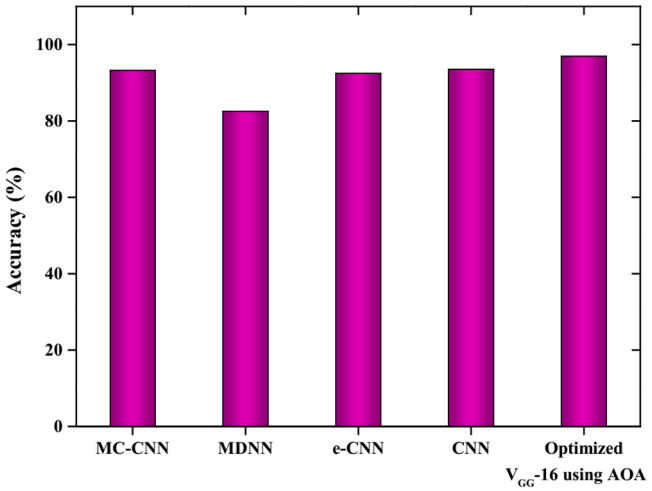

Fig. 10. State-of-art comparison of accuracy.

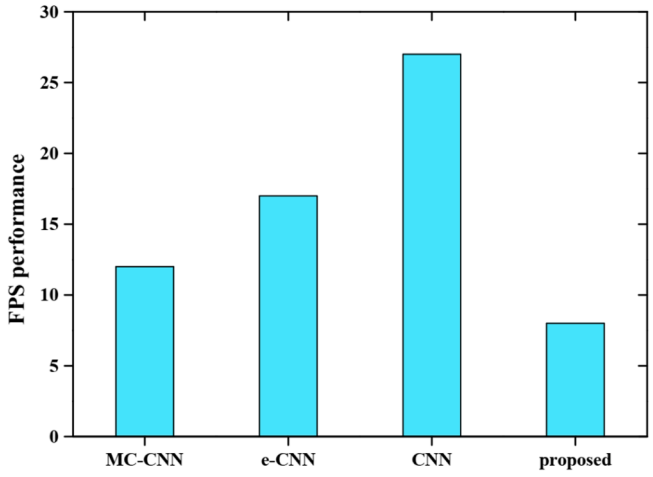

Fig. 11. State-of-art comparison of FPS.

Table 5
State-of-art comparison of classification.

Name of the methods	Evaluation measures				
	Specificity	Sensitivity	Precision	Recall	F-measure
MC-CNN	90.78%	91.12%	95.5%	89.4%	88.90%
MDNN	92.89%	92.45%	89.90%	88.72%	89.34%
e-CNN	90.56%	90.78%	88.92%	92.67%	90.35%
CNN	89.90%	93.20%	92.56%	93.56%	92.14%
DL	88.9%	94.12%	94.82%	94.23%	90.11%
Proposed	96.78%	96.21%	96.90%	95.82%	95.78%

$$F_{measure} = \frac{2 * P * R}{R + P} \tag{17}$$

where, T_{pos} - the classifier correctly classifies the affected region called a true positive.T_{neg} - the classifier correctly classifies the non-affected region called a true negative.F_{pos} - the classifier wrongly classifies the affected region called false positive.F_{neg} - the classifier wrongly classifies the non-affected region called a false negative.

4.3. Discussions

Table 4 summarizes the outcomes of the pre-processing. The training and testing rates are described with and without preprocessing. Fig. 4 describes the state-of-art result of segmentation. In this study, the segmentation techniques such as region-based segmentation, edge detection, thresholding-based segmentation, and adaptive ROI. In our study, we used an adaptive ROI segmentation model that provided better segmentation results than other existing studies such as region-based segmentation, edge detection, and thresholding-based segmentation.

In this study, the performance assessment with respect to accuracy and loss are delineated in Fig. 5. There are 100 epochs are used to evaluate the performance of accuracy and loss. The training and validation accuracy is delineated in Fig. 5(a). This investigation provides 0.97% training accuracy and 0.92% validation accuracy. Fig. 5(b) explains the training and validation losses. From this Fig. 5(b), the training and validation loss of 0.05% and 0.16% are obtained.

The confusion matrix assessment based on classification performance is depicted in Fig. 6. At the training stage, an optimized VGG-16 using the AOA model in the case of normal, mild dementia, and late dementia classes are assessed in this experiment. The blue color corresponding to the diagonal matrix expresses the accuracy of each relevant class.

The local and global optima performance analysis of AOA is depicted in Fig. 7. This investigation is performed between different numbers of generations and the objective values. The AOA effectively balances both global exploration and local exploitation capabilities, as shown in Fig. 7.

The performance assessment of various classes is delineated in Fig. 8. Three classes such as normal, mild dementia, and late dementia validate the performance of optimized VGG-16 using AOA for AD classification. The normal class demonstrated 97% accuracy, 92% specificity, and 95% specificity. Based on mild dementia, the outputs of 96% accuracy, 90% specificity, and 90% specificity are obtained. At last, the late dementia class delineated 95% accuracy, 94% specificity, and 92% specificity respectively.

The state-of-art comparison of classification based on the evaluation measures is illustrated in Fig. 9. The proposed optimized VGG-16 with AOA with AlexNet, InceptionV3, and GoogleNet, VGG-16. By using optimized VGG-16 with AOA, we have obtained 96%, 95.7%, and 95% performances with respect to normal, mild dementia, and late dementia classes.

The state-of-art comparison of accuracy is delineated in Fig. 10. The most recent work such as Multi-Modality Cascaded Convolutional Neural Networks (MC-CNN) [8], Multiscale Deep Neural Networks (MDNN) [9], ensemble system of deep convolutional neural networks (e-CNN) [10], convolutional neural networks (CNN) [13], and proposed an optimized VGG-16 using AOA methods are used in this study. According to this investigation, the accuracy of 93.26%, 82.51%, 92.48%, 93.5%, and 97% are obtained by using MC-CNN, MDNN, e-CNN, CNN, and the proposed method. The proposed optimized VGG-16 employing the AOA model outperformed previous approaches in terms of accuracy.

The state-of-art comparison of AD classification performance is delineated in Table 5. The existing methods such as with Multi-Modality Cascaded Convolutional Neural Networks (MC-CNN) [8], Multiscale Deep Neural Networks (MDNN) [9], ensemble system of deep convolutional neural networks (e-CNN) [10], convolutional neural networks (CNN) [13], and deep learning (DL) [12] with proposed an optimized VGG-16 using AOA model is used. Therefore, the proposed method delivered 96.78% specificity, 96.21% sensitivity, 96.90% precision, 95.82% recall, and 95.78% F-measure outputs. The MD-DNN dataset is not suited for other architectures and is incapable of detecting Alzheimer's disease in the different parts of the brain. However, the proposed method offered superior classification performances than other previous methods.

The state-of-the-art result of frame per second (FPS) with respect to CNN techniques such as Multi-Modality Cascaded Convolutional Neural Networks (MC-CNN) [8], ensemble system of deep convolutional neural networks (e-CNN) [10], convolutional neural networks (CNN) [13], and the proposed method is shown in Fig. 11. This investigation

demonstrated different performance results. However, the proposed method demonstrated 8 s FPS than other exiting techniques.

The drawbacks associated with the state-of-art techniques are presented here. The authors of the e-CNN and CNN architectures were unable to include data from several datasets, and the models also took longer to process. The performance of the CNN architecture is mainly decreased due to the higher computational cost and imbalanced data distributions. When compared to the existing works, our proposed method achieves less computational cost, lower processing time, higher detection accuracy and it has the ability to record brain-affected regions in which the proposed method is suitable for all AD datasets.

5. Conclusion

This study proposed an optimized VGG-16 using AOA for AD classification such as normal, mild dementia, and late dementia respectively. The implementation platform of python, Keras, and Tensor Flow on Linux X86-64 machine with NVIDIA GeForce GTX 770 is used to simulate the proposed model. Six evaluation measures with various kinds of experimental investigation, confusion matrix analysis, and state-of-art comparison are carried out. Based on the experimental investigation, the normal, mild dementia, and late dementia demonstrated superior performances in terms of accuracy, specificity, and sensitivity results. The proposed method offers 97% more accuracy than other existing methods including MC-CNN, MDNN, e-CNN, and CNN. When compared to the previous techniques, the proposed method demonstrated 96.78% specificity, 96.21% sensitivity, 96.90% precision, 95.82% recall, and 95.78% F-measure results. However, the proposed method outperformed superior performances than other previous models for AD classification. The proposed method provides a number of benefits, including improved classification results, lower computing costs, and faster execution time.

6. Authors' Contributions

Author contributions included conception and study design (ND and SPC), data collection or acquisition (ND and SPC), statistical analysis (ND and SPC), interpretation of results (ABD, DEF, GHI and MNO), drafting the manuscript work or revising it critically for important intellectual content (ND and SPC) and approval of final version to be published and agreement to be accountable for the integrity and accuracy of all aspects of the work (All authors).

CRediT authorship contribution statement

N. Deepa: Conceptualization, Methodology, Software. **S.P. Chokkalingam:** Writing – original draft, Investigation, Writing – review & editing.

Declaration of Competing Interest

The authors declare that they have no known competing financial interests or personal relationships that could have appeared to influence the work reported in this paper.

References

[1] C. Lian, M. Liu, J. Zhang, D. Shen, Hierarchical fully convolutional network for joint atrophy localization and Alzheimer's disease diagnosis using structural MRI, IEEE Trans. Pattern Anal. Mach. Intell. 42 (4) (2020) 880–893.

[2] G.M. McKhann, D.S. Knopman, H. Chertkow, B.T. Hyman, C.R. Jack Jr, C. H. Kawas, W.E. Klunk, W.J. Koroshetz, J.J. Manly, R. Mayeux, R.C. Mohs, The diagnosis of dementia due to Alzheimer's disease: recommendations from the National Institute on Aging-Alzheimer's Association workgroups on diagnostic guidelines for Alzheimer's disease, Alzheimer's & Dementia 7 (3) (2011) 263–269.

[3] J. Weller, A. Budson, Current understanding of Alzheimer's disease diagnosis and treatment. F1000Research, 7 (2018).

[4] R. Cassani, M. Estarellas, R. San-Martin, F.J. Fraga, T.H. Falk, Systematic review on resting-state EEG for Alzheimer's disease diagnosis and prgression assessment, Dis. Markers 2018 (2018).

[5] Y. Pan, M. Liu, C. Lian, T. Zhou, Y. Xia, D. Shen, D, Synthesizing missing PET from MRI with cycle-consistent generative adversarial networks for Alzheimer's disease diagnosis. In International Conference on Medical Image Computing and Computer-Assisted Intervention, 2018 (pp. 455-463). Springer, Cham.

[6] S. Esmaeilzadeh, D.I. Belivanis, K.M. Pohl, E. Adeli, in: End-to-end Alzheimer's disease diagnosis and biomarker identification, Springer, Cham, 2018, pp. 337–345.

[7] G.B. Frisoni, M. Boccardi, F. Barkhof, K. Blennow, S. Cappa, K. Chiotis, J.-F. Démonet, V. Garibotto, P. Giannakopoulos, A. Gietl, O. Hansson, K. Herholz, C. R. Jack, F. Nobili, A. Nordberg, H.M. Snyder, M. Ten Kate, A. Varrone, E. Albanese, S. Becker, P. Bossuyt, M.C. Carrillo, C. Cerami, B. Dubois, V. Gallo, E. Giacobini, G. Gold, S. Hurst, A. Lönneborg, K.-O. Lovblad, N. Mattsson, J.-L. Molinuevo, A. U. Monsch, U. Mosimann, A. Padovani, A. Picco, C. Porteri, O. Ratib, L. Saint-Aubert, C. Scerri, P. Scheltens, J.M. Schott, I. Sonni, S. Teipel, P. Vineis, P.J. Visser, Y. Yasui, B. Winblad, Strategic roadmap for an early diagnosis of Alzheimer's disease based on biomarkers, Lancet Neurol. 16 (8) (2017) 661–676.

[8] M. Liu, D. Cheng, K. Wang, Y. Wang, Multi-modality cascaded convolutional neural networks for Alzheimer's disease diagnosis, Neuroinformatics 16 (3-4) (2018) 295–308.

[9] D. Lu, K. Popuri, G.W. Ding, R. Balachandar, M.F. Beg, Alzheimer's Disease Neuroimaging Initiative. Multiscale deep neural network based analysis of FDG-PET images for the early diagnosis of Alzheimer's disease, Med. Image Anal. 46 (2018) 26–34.

[10] J. Islam, Y. Zhang, Brain MRI analysis for Alzheimer's disease diagnosis using an ensemble system of deep convolutional neural networks, Brain Informatics 5 (2) (2018) 1–14.

[11] M. Liu, J. Zhang, E. Adeli, D. Shen, D, Joint classification and regression via deep multi-task multi-channel learning for Alzheimer's disease diagnosis, IEEE Trans. Biomed. Eng. 66 (5) (2019) 1195–1206.

[12] A. Puente-Castro, E. Fernandez-Blanco, A. Pazos, C.R. Munteanu, Automatic assessment of Alzheimer's disease diagnosis based on deep learning techniques, Comput. Biol. Med. 120 (2020), 103764.

[13] E.N. Marzban, A.M. Eldeib, I.A. Yassine, Y.M. Kadah, S.D. Ginsberg, Alzheimer's Disease Neurodegenerative Initiative. Alzheimer's disease diagnosis from diffusion tensor images using convolutional neural networks, PLoS One 15 (3) (2020) e0230409, https://doi.org/10.1371/journal.pone.0230409.

[14] D. Pan, A. Zeng, L. Jia, Y. Huang, T. Frizzell, X. Song, Early detection of Alzheimer's disease using magnetic resonance imaging: a novel approach combining convolutional neural networks and ensemble learning, Front. Neurosci. 14 (2020).

[15] A. Mehmood, M. Maqsood, M. Bashir, Y. Shuyuan, A deep Siamese convolution neural network for multi-class classification of Alzheimer disease, Brain sciences 10 (2) (2020) 84.

[16] M. Usman, B.D. Lee, S.S. Byon, S.H. Kim, B.I. Lee, Y.G. Shin, Volumetric lung nodule segmentation using adaptive roi with multi-view residual learning, Sci. Rep. 10 (1) (2020) 1–15.

[17] Z. Zhang, Q. Liu, Y. Wang, Road extraction by deep residual u-net, IEEE Geosci. Remote Sens. Lett. 15 (5) (2018) 749–753.

[18] D. Alvarez-Marin, K.S. Ochoa, Indexical cities: articulating personal models of urban preference with geotagged data. arXiv preprint arXiv:2001.10615 (2020).

[19] C. Szegedy, V. Vanhoucke, S. Ioffe, J. Shlens, Z. Wojna, Rethinking the inception architecture for computer vision. In Proceedings of the IEEE conference on computer vision and pattern recognition 2016, pp. 2818-2826.

[20] D. Xu, C. Doutre, P. Nasiopoulos. Saturated-pixel enhancement for color images. In Proceedings of 2010 IEEE International Symposium on Circuits and Systems 2010, pp. 3377-3380, IEEE.

[21] A. Acevedo, S. Alférez, A. Merino, L. Puigví, J. Rodellar, Recognition of peripheral blood cell images using convolutional neural networks, Comput. Methods Programs Biomed. 180 (2019), 105020.

[22] S. Mirjalili, SCA: a sine cosine algorithm for solving optimization problems, Knowl.-Based Syst. 96 (2016) 120–133.

[23] L. Abualigah, A. Diabat, S. Mirjalili, M. Abd Elaziz, A.H. Gandomi, The arithmetic optimization algorithm, Comput. Methods Appl. Mech. Eng. 376 (2021) 113609.

[24] M. Toğaçar, B. Ergen, Z. Cömert, COVID-19 detection using deep learning models to exploit Social Mimic Optimization and structured chest X-ray images using fuzzy color and stacking approaches, Comput. Biol. Med. 121 (2020) 103805, https://doi.org/10.1016/j.compbiomed.2020.103805.

[25] D. Ezzat, A.E. Hassanien, H.A. Ella, An optimized deep learning architecture for the diagnosis of COVID-19 disease based on gravitational search optimization, Appl. Soft Comput. (2020), 106742.

[26] F. Li, M. Liu, Alzheimer's Disease Neuroimaging Initiative. Alzheimer's disease diagnosis based on multiple cluster dense convolutional networks, Comput. Med. Imaging Graph. 70 (2018) 101–110.

[27] E. Hosseini-Asl, R. Keynton, A. El-Baz, Alzheimer's disease diagnostics by adaptation of 3D convolutional network. In 2016 IEEE International Conference on Image Processing (ICIP), 2016, pp. 126-130. IEEE.

[28] K. Bäckström, M. Nazari, I.Y.H. Gu, A.S. Jakola, An efficient 3D deep convolutional network for Alzheimer's disease diagnosis using MR images. In 2018 IEEE 15th International Symposium on Biomedical Imaging (ISBI 2018), 2018, pp. 149-153. IEEE.

[29] J. Rieke, F. Eitel, M. Weygandt, J.D. Haynes, K. Ritter, in: Visualizing convolutional networks for MRI-based diagnosis of Alzheimer's disease, Springer, Cham, 2018, pp. 24–31.

[30] H. Yu, L. Zhu, L. Cai, J. Wang, J. Liu, R. Wang, Z. Zhang, Identification of Alzheimer's EEG with a WVG network-based fuzzy learning approach, Front. Neurosci. 14 (2020) 641.
[31] H. Yu, X. Lei, Z. Song, C. Liu, J. Wang, Supervised network-based fuzzy learning of EEG signals for Alzheimer's disease identification, IEEE Trans. Fuzzy Syst. 28 (1) (2020) 60–71.
[32] K. Li, J. Wang, S. Li, H. Yu, L. Zhu, J. Liu, L. Wu, Feature extraction and identification of Alzheimer's disease based on latent factor of multi-channel EEG, IEEE Trans. Neural Syst. Rehabil. Eng. 29 (2021) 1557–1567.
[33] H. Yu, X. Wu, L. Cai, B. Deng, J. Wang, Modulation of spectral power and functional connectivity in human brain by acupuncture stimulation, IEEE Trans. Neural Syst. Rehabil. Eng. 26 (5) (2018) 977–986.
[34] H. Yu, X. Li, X. Lei, J. Wang, Modulation effect of acupuncture on functional brain networks and classification of its manipulation with EEG signals, IEEE Trans. Neural Syst. Rehabil. Eng. 27 (10) (2019) 1973–1984.
[35] S. Duchesne, I. Chouinard, O. Potvin, V.S. Fonov, A. Khademi, R. Bartha, P. Bellec, D.L. Collins, M. Descoteaux, R. Hoge, C.R. McCreary, The Canadian dementia imaging protocol: harmonizing national cohorts, J. Magn. Reson. Imaging 49 (2) (2019) 456–465.
[36] V. Sundararaj, M. Selvi, Opposition grasshopper optimizer based multimedia data distribution using user evaluation strategy, Multimedia Tools Appl. 80 (19) (2021) 29875–29891.
[37] J. Jose, N. Gautam, M. Tiwari, T. Tiwari, A. Suresh, V. Sundararaj, M.R. Rejeesh, An image quality enhancement scheme employing adolescent identity search algorithm in the NSST domain for multimodal medical image fusion, Biomed. Signal Process. Control 66 (2021) 102480.
[38] V. Sundararaj, Optimised denoising scheme via opposition-based self-adaptive learning PSO algorithm for wavelet-based ECG signal noise reduction, Int. J. Biomed. Eng. Technol. 31 (4) (2019) 325–345.
[39] V. Sundararaj, An efficient threshold prediction scheme for wavelet based ECG signal noise reduction using variable step size firefly algorithm, Int. J. Intell. Eng. Syst. 9 (3) (2016) 117–126.
[40] B.A. Hassan, T.A. Rashid, H.K. Hamarashid, A novel cluster detection of COVID-19 patients and medical disease conditions using improved evolutionary clustering algorithm star, Comput. Biol. Med. 138 (2021) 104866.